OXFORD Toxicology Research

Toxicology Research, 2020, **9**, 308–322

doi: 10.1093/toxres/tfaa025
Advance Access Publication Date: 21 May 2020
Paper

PAPER

Investigation of hypoglycemic effects, oxidative stress potential and xanthine-oxidase activity of polyphenols (gallic acid, catechin) derived from faba bean on 3T3-L1 cell line: insights into molecular docking and simulation study

Dhiraj Kumar Choudhary,[1] Navaneet Chaturvedi,[1] Amit Singh[2] and Abha Mishra[1,*]

[1]Biomolecular Engineering Laboratory, School of Biochemical Engineering, Indian Institute of Technology, Banaras Hindu University, Varanasi 221005, India, and [2]Department of Pharmacology, Institute of Medical Sciences, Banaras Hindu University, Varanasi 221005, India

*Correspondence address. Biomolecular Engineering Laboratory, School of Biochemical Engineering, Indian Institute of Technology, Banaras Hindu University, Varanasi 221005, India. E-mail: abham.bce@itbhu.ac.in.

Abstract

Hypoglycemic potential and xanthine-oxidase (XO) activity of polyphenols from faba bean were evaluated in the 3T3-L1 cell line, and an interaction study *in silico* with XO was performed with considerable bioactive components of acetone extract of faba beans. The protonated and fragmented behavior of acetone seed extract revealed the presence of gallic acid (MS/MS, m/z 169) and catechin (MS^n, m/z 288.3). Flow cytometry study explained the effect of hydrogen peroxide (H_2O_2) on cell line as cell death was increased from 9.72 to 41.66% as compared to the control (without H_2O_2). The atomic force microscopy (AFM), scanning electron microscopy and reactive oxygen species measurement also confirmed the protective effect of polyphenols in the 3T3-L1 cell lines. Oxidative stress through propidium iodide and 4′,6-diamidino-2-phenylindole staining demonstrated that the apoptotic ratio was 0.35 ± 2.62 ($P < 0.05$) and 30 ± 2.54% in H_2O_2-treated cells, respectively, as compared to control. The observations of flow cytometry and confocal microscopy marked the effect of seed extract (0.86 ± 0.031, 3.52 ± 0.52, $P < 0.05$), on glucose uptake in cells through the better relative fluorescence intensity than that of the control. Moreover, molecular docking and molecular dynamics simulation studies gave an insight into the predicted residues that hold favorable polyphenolic-specific interactions. The probable binding modes of the gallic acid and catechin from this study may extend the knowledge of the XO-polyphenol interactions and offered the way to design the analogs of acetone seed extract with reduced toxicity.

Key words: catechin, gallic acid, xanthine-oxidase, flow cytometry, confocal microscopy, molecular dynamic simulation

Received: 21 December 2019; **Revised:** 24 March 2020; **Accepted:** 1 April 2020

Introduction

Oxidative stress results in the unnecessary development of reactive oxygen species (ROS).

The growth of insulin resistance, β cell failure, compromised glucose tolerance and type 2.

Diabetes mellitus is responsible for oxidative stress [1–2]. Free radical production is regulated by the antioxidant defense system, but polyphenols (gallic acid, ellagic acid, catechin, epicatechin) are likely to neutralize excessive free radical generation owing to antioxidant properties. Recently, there has been a growing interest in the beneficial effects of dietary polyphenols on the prevention of chronic diseases, including obesity, diabetes and other diseases. Highly rich in polyphenols such as flavonoids, terpenoids and other constituents are accountable for diminishing the blood glucose levels [3–4]. Phenolic compounds gain more interest in phytochemicals as a result of their health [5].

In faba beans, polyphenols are found in several parts of the plant [6]. Faba beans (*Vicia faba*) have a range of bioactive components such as ellagic acid, gallic acid, ellagitannins, and gallotannins and are widely known for their antioxidant, antidiabetic and antibacterial pharmacological impact [7]. Recently, the anti-diabetic potential of polyphenols had been linked to reducing oxidative stress in experimental diabetes by Sabu *et al.* [8]. Xanthine-oxidase (XO) can be taken as a biomarker of oxidative stress in diabetes mellitus patients [9]. The antioxidant function is an important key for the assessment of oxidative stress and diabetes mellitus *in vitro* as a possible therapeutic use of polyphenols. Polyphenols such as gallic acid, ellagic acid, catechin, epicatechin, butein, fisetin, diosmetin, tricetin, genistein, tricin, vitexycarpin, herbacetin, biochanin, rhamnetin, and isorhamnetin exert XO inhibition activity [10]. Benzopyrene ring is known to contribute to its XO inhibitory function in the core nucleus of polyphenols [11]. Out of many secondary plant metabolites, the group of polyphenols might be most hopeful due to its well-recognized antioxidative and gene regulatory properties [12]. Polyphenols are competent to act anti-inflammatory both *in vitro* and *in vivo* by inhibiting the activation of nuclear factor kappa B (NF-jB) and to induce antioxidative and cytoprotective effects by inducing nuclear factor erythroid 2-related factor-2 (Nrf2) [13]. It was reported in cell culture studies that ROS has a connecting relationship with insulin resistance, which is a key feature of diabetes mellitus type-II [14]. Besides, molecular docking and MD simulation with ligands (gallic acid, catechin) with XO were performed to predict actions utilizing conformational changes. A temporal distribution study is provided to explain the clusters that were characterized by a conformation, each persisting longer time, suggesting regular progress towards a stable relaxed state of the complex. An explanation of the representative structure of the largest cluster is provided by means of the electrostatic shell. The present study focuses on the assessment of antidiabetic and antioxidant properties of faba bean seed extract and the effect of extracted polyphenols on XO.

Materials and Methods

Chemicals and reagents

(2-(N-(7-Nitrobenz-2-oxa-1,3-diazol-4-yl)Amino)-2-Deoxy-D-glucose) (2-NBDG) and Aldrich) and 2′,7′ dichlorodihydrofluorescein diacetate were bought from Sigma-Aldrich, USA. Propidium iodide (PI), DAPI, dexamethasone, oil red, 4′,6′- diamidino-2 phenylindole dye (DAPI), Dulbecco's modified eagle medium (DMEM) (Himedia, India), fetal bovine serum (FBS), 3-and (4,5-dimethylthiazol-2-yl)-2,5-diphenyltetrazolium bromide (MTT,) penicillin and streptomycin antibiotics were also purchased from Himedia, India. Other reagents were of high purity and analytical quality.

Seed material and preparation of seed extract

Vikrant bean variety (*Vicia faba* L.) was collected from the National Plant Genetic Resources Bureau (NBPGR) New Delhi, India. Sequential extraction was performed for polyphenols extraction from the bean. The extraction of polyphenols was carried out using acetone, methanol, ethanol and water. In 100 ml of solvent, fine powdered bean samples (40 g) were applied and held under shaking at 130 rpm for temperature 40°C. Samples were centrifuged at 4000 rpm for 20 min at 37°C temperature. The supernatant was collected, the precipitate resuspended in the second solvent and kept for 48 h under shaking at 130 rpm at temperature 40°C and again centrifuged at 4000 rpm. The supernatants were combined and concentrated under reduced pressure at 40°C. Dried concentrated extracts were stored in the refrigerator at 4°C.

Column chromatography

Gradient fractionation of seed extract (from the acetone seed extract) was performed by eluting the column with toluene:ethyl acetate:methanol (4:3:3) accompanied by acetone over silica gel resulting in the isolation of compounds designated as D1 (05) (gallic acid), D2 (08) (catechin) and from fractions 5 and 8, respectively.

Mass spectrometry

Mass spectrometry with MSn data-dependent mode is a quick and reliable method for confirming unknown compound structures. Mass spectra were obtained with an Linear Trap Quadropole (LTQ) linear ion trap tandem mass spectrometer (Thermo Electron, San Jose, CA, USA), equipped with an atmospheric pressure ionization interface. The spectra were observed in direct infusion mass (MS, MS/MS, MS^n) with Negative Electrospray Ionization (ESI) mode. Mass ranging was varying from the thin range such as 50–2000 m/e. Under automated conditions of gain control, data-dependent experiments are carried out. This method is generally useful for information on the molecular weight of unknown compounds. Data-dependent experiments were performed under automatic gain-control conditions. This technique is generally useful for information on the molecular weight of compounds. This technique was used to classify drug metabolites in complex biological matrices [15] and also used for the identification of polyphenols [16].

Xanthine oxidase inhibitory assay

In vitro interaction of xanthine oxidase with faba bean was already reported by Choudhary & Mishra [17].

Cell culture and differential assay

The 3T3-L1 cell line of mouse muscle fibroblasts was bought from NCCS, Pune, India. The 3T3-L1 preadipocytes culture and differentiation protocol were described previously [18]. Cells were cultured and maintained in DMEM containing 10% FBS, and 100 µl/ml streptomycin, 100 U/ml penicillin with 5% CO_2 at 37°C

constant temperature in CO_2 incubator. After 80% confluence, the cells were transferred to the differential medium, 0.5 mM of methyl isobutyl xanthine, 0.25 µM of dexamethasone, DMEM containing 10% FBS and 1 µg/ml of insulin for 2 days. After that, cells were incubated in DMEM containing 10% FBS and insulin (1 µg/ml) for 2 days. Later, the cells were subcultured in 10% FBS-DMEM.

Oil red O staining

The 3T3-L1 confluent cells (80%) were washed two times with phosphate buffer solution (PBS) and then fixed for 1 h at room temperature with 10% formalin, prepared in PBS. At that point, cells were washed two times with PBS. Then, cells were washed with PBS and stained with a filtered oil red solution (0.5% in 60% isopropanol) for 1 h. At last, cells were washed twice with distilled water.

MTT assay

Cell viability of 3T3-L1 preadipocytes was followed using 3-(4,5-dimethylthiazol-2-yl)-2,5-diphenyltetrazolium bromide (MTT) assay. First of all, preadipocytes cells (1×10^4 cells/well) were seeded out in 96-well-tissue plates properly and cultured for 3 days. Then, the cells were washed once in PBS and treated with 1.0 mg/ml concentrations of different seed extracts (0.5 mg/ml) and incubated for 24 h. All the seed extract samples were removed, and 10 µl of MTT solution (0.5 mg/ml) was added to each well. Cells were treated with different faba bean seed extracts and incubated at 37°C for 1 h in 96-well plates. Finally, 150 µl DMSO (0.1–0.5%) was added to dissolve the formazan crystals. Absorbance was evaluated by a spectrophotometer at 540 nm.

ROS evaluation by DCF-DA (2′,7′-dichlorofluorescein diacetate) assay

This method is extensively applied to profile the oxidative status of living cells [19]. 3T3-L1 cells (1×10^4 cells) were treated with (i) H_2O_2, (ii) insulin, (iii) extract independently and incubated at 37°C in CO_2 for 1 h, then all samples were washed with PBS and 20 µM H2DCFDA was added. Air drying was done for 1 h at room temperature. Cells were analyzed using the LSM510 confocal microscopy (Zeiss, Jena, Germany).

Oxidative stress study via flow cytometry approach

Trypsinization method was utilized to harvest treated and untreated cells and washed with phosphate buffer saline and resuspended the pellet in 100 1× PBS. About 10–20 µl of PI staining solution was added to each sample. The same volume was maintained for all samples, mixed gently and incubated for 1 min in a dark environment. PI fluorescence was determined with FACS scan™ using FL-2 or FL-3 channel. Data were acquired for unstained and single positive control. Stop count was fixed on the viable cells from the dot plot of forward scatter, and red fluorescence FL-2 channel with 585/42 nm band-pass filter was observed. The compensations and the settings had been adjusted according to the protocol. Data were analyzed with the use of BD Cell Quest Pro software.

DAPI staining

DAPI staining protocol was followed by the modified procedure [20]. About, 3% paraformaldehyde was applied for the fixation of control and treated cells. Cells were permeabilized with 0.2% Triton X-100 in phosphate-buffered saline (PBS). About 20 µl of 5 mg/ml of DAPI was added into each sample and air-dried. Then samples were visualized by ZEISS LSM780 confocal microscopy.

PI staining

PI staining protocol was used to differentiate apoptotic cells from normal cells, which displays nuclear changes during apoptosis [21]. 3T3-L1 cells were treated at a density of 1×10^4 cells/mL with H_2O_2 and extract for 1 h at 37°C. It was permeabilized with a combination of acetone:methanol (1:1) at 37°C for 10 min. Then, PI (10 µl) was added to each sample and fixation was done by air. It was observed under ZEISS LSM780 confocal microscopy.

Atomic force microscopy

The primary point of utilizing this technique was to know the impact of hydrogen peroxide (H_2O_2) and seed extract on cells in terms of cell roughness. (H_2O_2 is regularly utilized used as the source of oxygen-derived free radicals. Control (1×10^4 cells) and treated cells (1×10^4 cells) were visualized under AFM model-Nt-Mdt, Russia for the surface morphological changes. The cell samples had been scanned in semi-contact modes, and experiments were accomplished in the air at room temperature [22]. The air-drying was executed to immobilize cells on the slide.

Oxidative stress through scanning electron microscopy

Scanning electron microscope (SEM) is commonly used to study structural features on the surface of biological samples. The traditional specimen preparation method for SEM consists of fixation, oxidation, drying and, optionally, conductive coating. Cells were cultured at 37°C and 5% CO_2 in DMEM supplemented with 10% FBS. Sterile coverslip per well was inserted in six-cell-well plates. 1×10^4 cells were then treated with extract and H_2O_2 for 60 min at 37°C. Then, primary fixation of cells was performed with freshly made 3.0% glutaraldehyde or/and 0.1% glutaraldehyde in PBS for 20 min at room temperature. Secondly, post-fixation step was done by 1% OsO_4 in osmium tetroxide (OsO_4). The samples were then dehydrated by a graded series of ethanol (50, 60, 70, 80, 90, 95% and three times 100%) at 20-min intervals. Following dehydration, the solvent was removed by either air drying with hexamethyldisilazane (HMDS). For HMDS drying, the dehydrated specimens were immersed with HMDS for 20 min. Then, HMDS was decanted, and the samples were left under a hood to air-dry at room temperature. Optionally, the conductive coating was performed. SEM model was EVO—SEM MA15/18 (CARL ZEISS microscopy).

Estimation of glucose uptake study in 3T3-L1 cells by confocal microscopy

Cultures were grown until 80% confluent where the medium was removed, and culture plates were rinsed three times in a phosphate buffer. Cover slips were put on six-well microtiter well plate. Cells (1×10^4) were then incubated at 37°C with 200 µM 2-NBDG and extract in the presence of phosphate buffer.

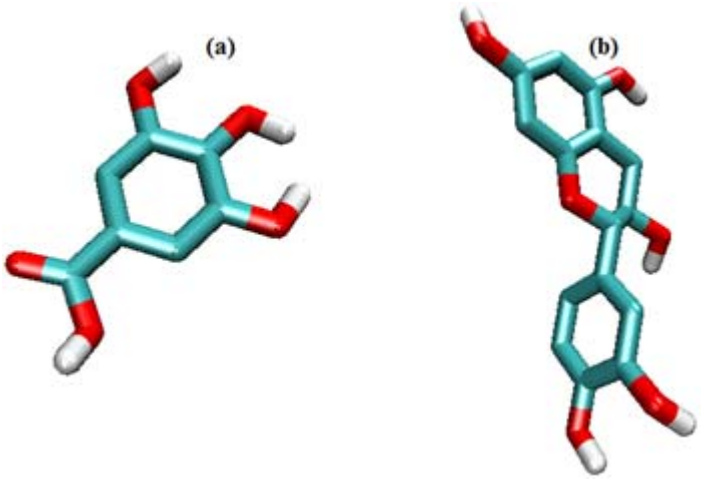

Figure 1: Visualization of the structure of **(a)** gallic acid and **(b)** catechin.

After 1 h, buffers were removed. Cells on slides were rinsed in Dulbecco's PBS and then fixed for 10 min in 4% paraformaldehyde. Cells were examined with a ZEISS LSM-780 confocal microscope. Image J software was used for fluorescence intensity (FI) measurement.

Glucose uptake assay by flow cytometry

The glucose uptake assay was performed as previously described with slight modification [23]. Briefly, cells were seeded in six-well plates at a density of 1×10^4 cells/well and incubated overnight. The medium was then replaced with the glucose- and serum-free DMEM containing insulin (100 nM), the fluorescent glucose analog 2-deoxy-2-[(7-nitro-2,1,3-benzoxadiazol-4-yl)amino]-D-glucose (2-NBDG, 10 µM) and samples (50 µM). After incubation for 24 h, the medium was removed and cells were washed with phosphate-buffered saline (PBS) twice. Cells were scraped out in 1 ml of PBS and transferred into 5-ml polystyrene round-bottom tubes (BD Falcon) and kept at 4°C. The amount of 2-NBDG taken up by the cells was measured in the FL1 channel using an FACS Calibur flow cytometer (BD Bioscience, San Jose, CA). Data from 10 000 single-cell events were collected. Values of relative FI were calculated as $FI = F_{I2\text{-}NBDG} - F_{Ibackground,}$ where $F_{I2\text{-}NBDG}$ is the FI of a single cell treated with or without the sample in the presence of 2-NBDG and $FI_{background}$ is the FI in the absence of 2-NBDG. Relative FI was calculated using image J software.

Molecular docking

The catechin [CID73160] and gallic acid [CID370] compounds (Fig. 1) were docked on the crystal structure of XO (PDB ID: 1FIQ) [24] using AutoDock 4.2 [25]. The numbers of grid points in *x*, *y*, *z* were set to 70, 70, 70, respectively, with the spacing value equivalent to 0.375 Å. Blind docking was performed where the number of docking runs was 150. The population in the genetic algorithm was 50, the number of energy evaluations was 250 000 and the maximum number of iterations was 27 000. Other parameters were set at the default values of the program.

Molecular dynamics simulation

System building. GROMACS 4.6.7 packages [26–27]were used for preparing the system and performing MD simulations using the gromos53a6 force field [28]. The protein solute was solvated by explicit SPC216 water [29] in a dodecahedron box with a margin of 10 Å between solute and the box walls. Systems were brought to neutrality by the addition of sodium counter ions.

Simulation detail. A 1-nm cut-off distance was taken under the particle-mesh Ewald method [30] to calculate long-range electrostatic interactions, and 1-nm cut-off distance was also considered to evaluate the van der Waals interactions. The LINCS algorithm of fourth-order expansion was used to constrain bond lengths [31]. The steepest-descent algorithm was applied to optimize for 10 000 steps to remove steric clashes between atoms. The system was equilibrated for 1 ns with position restraints of all heavy atoms. Berendsen weak coupling schemes were used to maintain the system at 300 K and 1 atom using separate baths for the system. Initial velocities were generated randomly using a Maxwell–Boltzmann distribution corresponding to 300 K. Finally, the production run was performed for 20 ns. Furthermore, xmgrace (http://plasma-gate.weizmann.ac.il) was used for preparing graphs. PyMol (The PyMOL Molecular Graphics System, Version 1.7 Schrödinger, LLC) packages were applied for a system inspection. Moreover, ligand topology preparation was implemented by using the PRODRG server with the option of choosing no chirality, full charge and no energy minimization [32].

Trajectory analysis. The g_rms tool of the GROMACS package was used to calculate the root-mean-square deviation (RMSD) of each trajectory. The equilibrated structure obtained after equilibration was considered as the reference structure, and the trajectories were fitted to the backbone of this structure. Temporal distribution was approximated using the g_cluster tool.

Statistical analysis

The entire experimental observations were carried out in triplicate, and the outcomes were expressed in terms of means ± standard deviation (n = 3). Graph Pad Prism 5.0 was used to evaluate the analysis of variance to compare the means, and differences were calculated as statistically significant at $P < 0.05$.

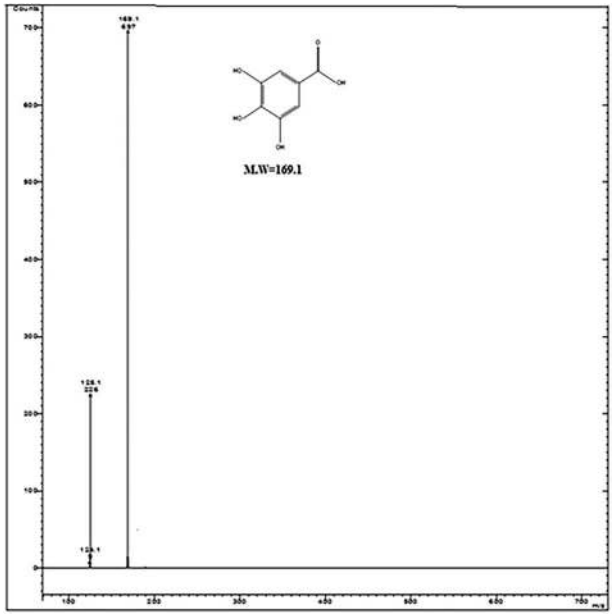

Figure 2: Mass spectra of fraction 8 (acetone seed extract) as molecular weight represents fragmentation pattern of catechin (288.3 → 269.3 → 246.3 → 241.1 → 213.3 → 203 → 187.2 → 115.2) in the negative ESI mode.

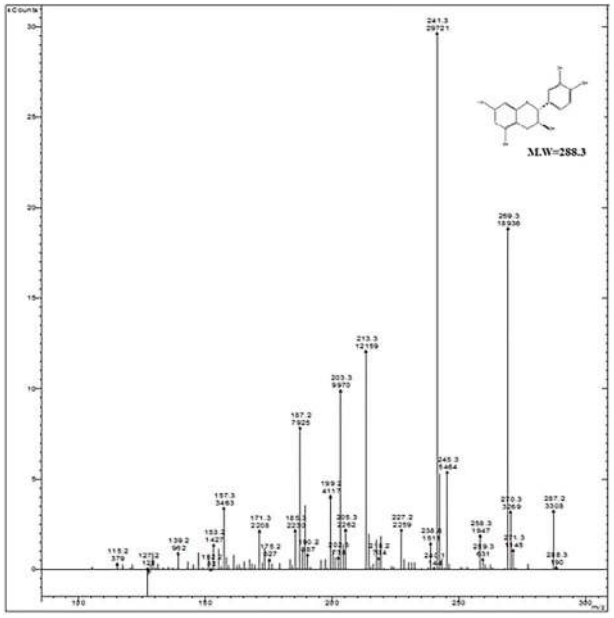

Figure 3: Mass spectra of fraction 5 (acetone seed extract) represent the fragmentation pattern of gallic acid (169.1 → 125.1) in the negative ESI mode.

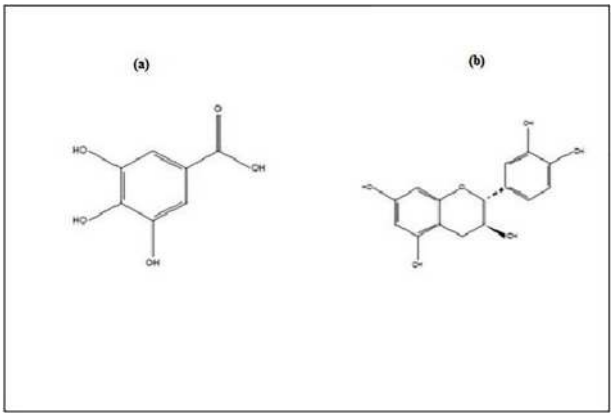

Figure 4: Structure of (**a**) gallic acid (**b**) catechin.

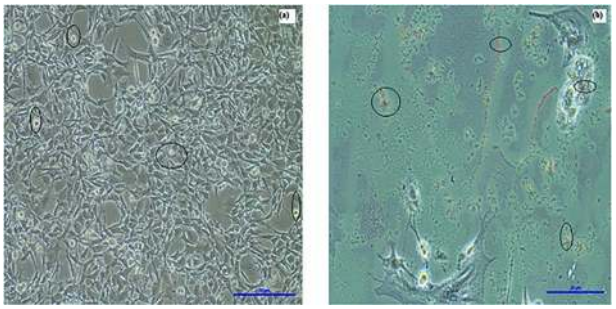

Figure 5: Phase-contrast microscopic observation: (**a**) circle represents lipid droplet after differentiation assay and (**b**) spherical red color shows the presence of oil or lipid droplet after 24 h.

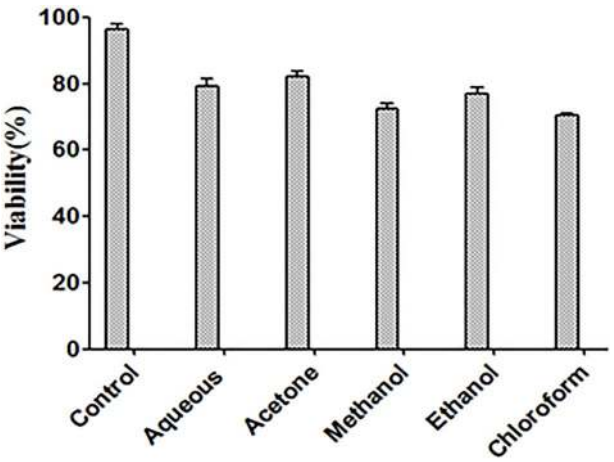

Figure 6: MTT assay represents the effect of different seed extracts on cell viability with respect to control.

Results and Discussion

Mass spectrometry

The protonated and fragmented ions of MS/MS of the m/z 169 (fraction 5) ion showed fragment ion at m/z 125.1. Abundant [M + H] + ions as the base peaks were formed in fraction 8. Their fragmentation pattern and molecular weight of fractions 5 and 8 showed the presence of gallic acid and catechin in faba bean seed extract [33]. The mass spectrum of fractions 6 and 8 was represented in Figs 2 and 3. The molecular structure of gallic acid and catechin were predicted in Fig. 4.

Cell differentiation study

The 3T3-L1 preadipocytes appeared to have a fusiform and flattened morphology, and some cells converted into a "rounded-up" morphology after initial 24 h of observation (Fig. 5). The fat droplets in 3T3-L1 cells were observed by phase-contrast microscope (Fig. 5). Lipid droplets were visualized by oil red O staining under phase-contrast microscope. Their size and numbers were gradually increased in a differentiating time-dependent manner. Cells were differentiated into 3T3-L1 adipocytes, which

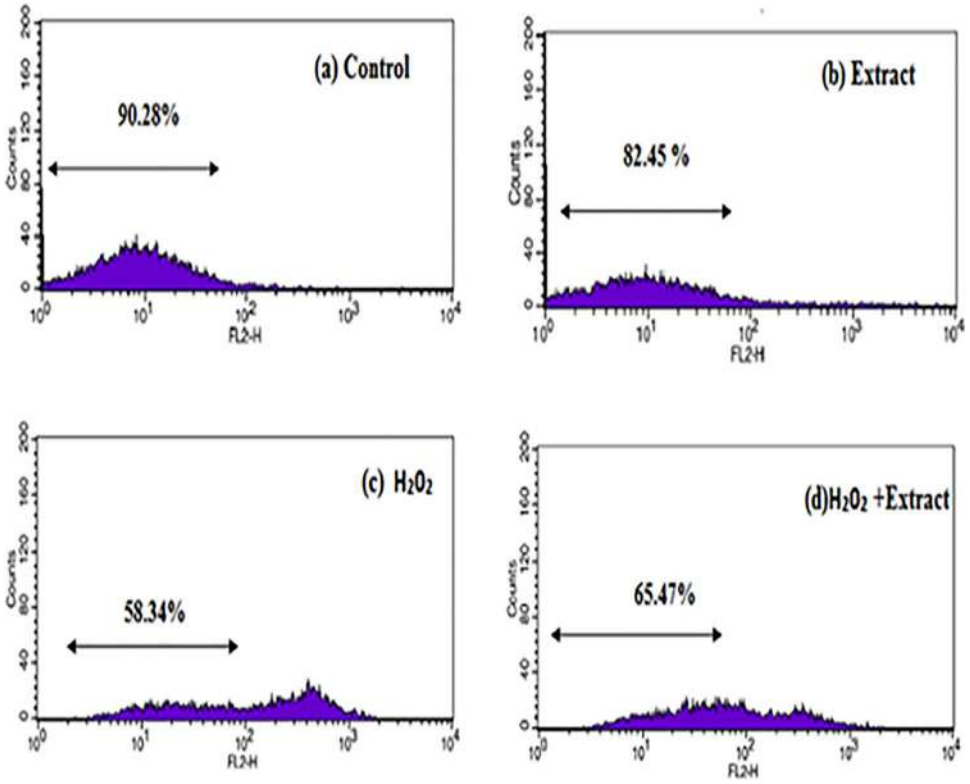

Figure 7: (**a**) Control, (**b**) extract, (**c**) H_2O_2 and (**d**) extract + H_2O_2 left side in image represent live cells and right side dead cells (flow cytometry).

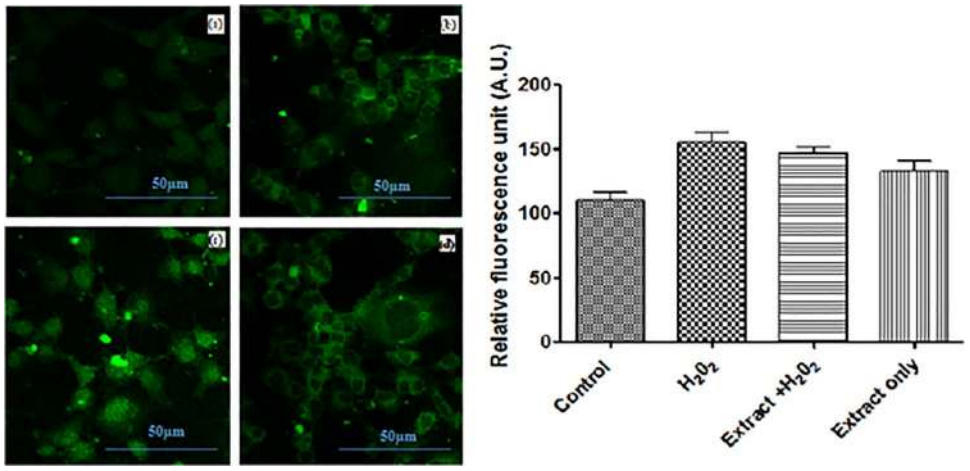

Figure 8: Measurement of ROS level by confocal microscopy: (**a**) control, (**b**) H_2O_2, (**c**) extract and (**d**) extract + H_2O_2 (right side of image relative FI measured by image J software).

revealed features of adipose cells, counting the expression of lipid metabolic genes and the production of lipid droplets [34].

Cell viability study

The maximum survival rate was found in acetone seed extract (87.067%, $P < 0.05$) as compared to control (97.36%., $P < 0.05$), and chloroform seed extract had the least survival potential (75.48%, $P < 0.05$) (Fig. 6). Figure 6 showed that there was a significant difference ($P < 0.05$) in the percentage of viable cells when treated with acetone extract when in comparison with the percentage of viable cells of the negative control (untreated) (97.36%, $P < 0.05$). Literature also authenticated that acetone extract is effective for cell survival [35].

Investigation of oxidative stress study by flow cytometry approach

Antioxidant properties of polyphenols, as suggested in the literature, may contribute to the protection of 3T3-L1 cells from oxidative stress-induced by H_2O_2 [36]. H_2O_2 exposure increased the apoptosis rate of 3T3-L1 cells from 9.72 to 41.66% compared to the control, which was declined to 17.55–34.53%, respectively, by extract and combination with H_2O_2 treatment (Fig. 7). The result

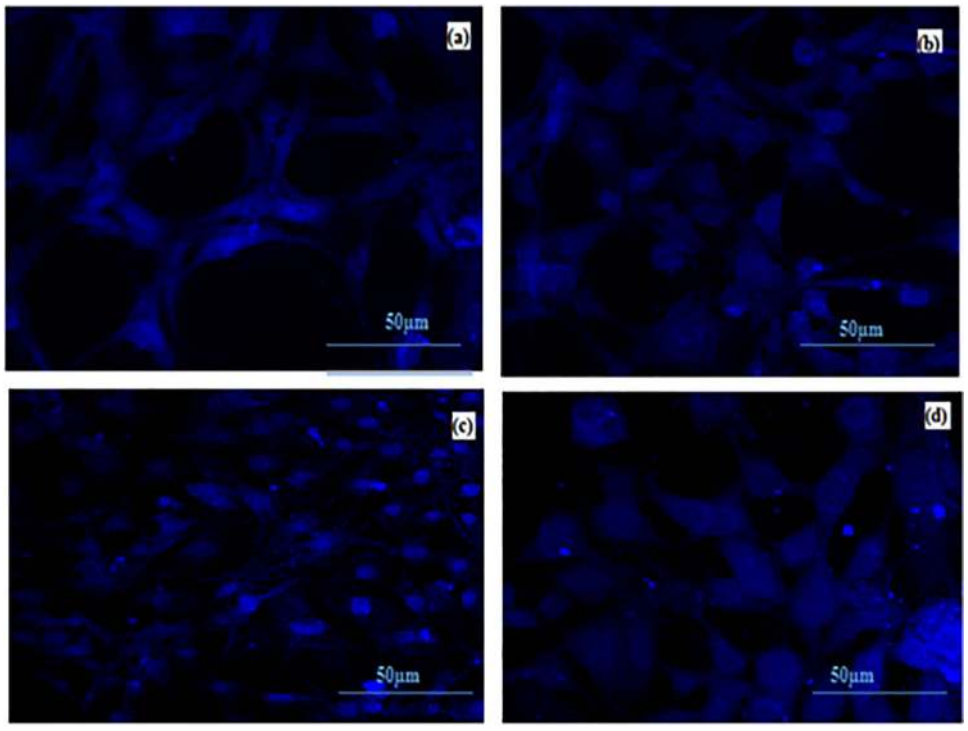

Figure 9: DAPI staining (confocal microscopy) showing oxidative stress effect of seed extract and H_2O_2 on yeast cells nuclei. (**a**) Control, (**b**) extract, (**c**) H_2O_2 and (**d**) H_2O_2 + extract.

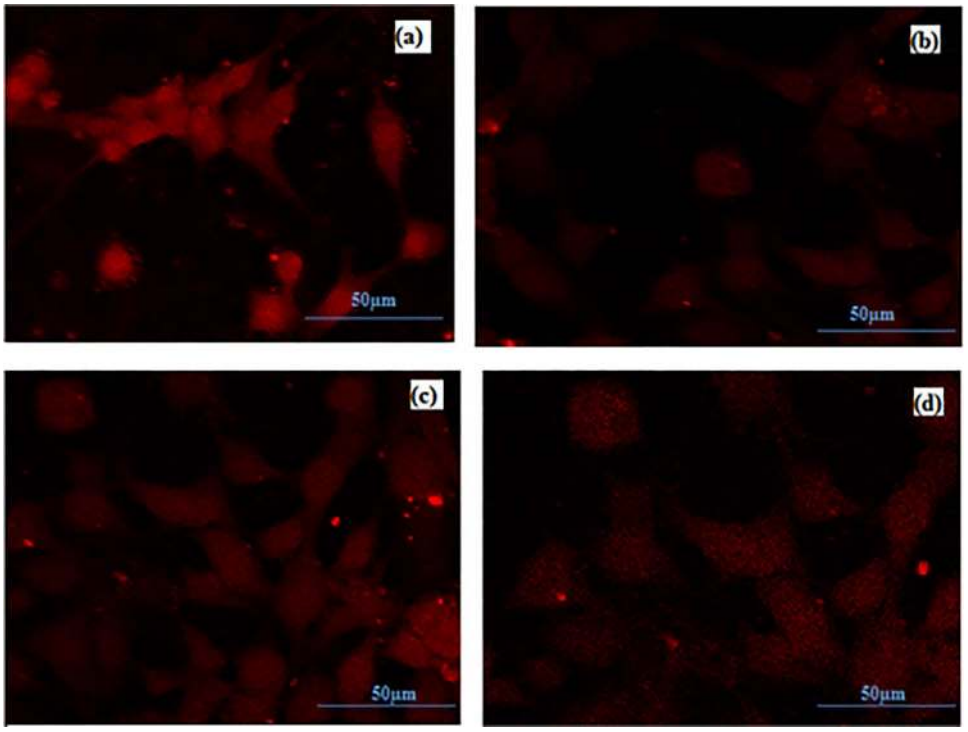

Figure 10: PI staining (confocal microscopy) showing oxidative stress effect of seed extract and H_2O_2 on 3T3-L1 cell population. (**a**) Control, (**b**) extract, (**c**) H_2O_2 and (**d**) H_2O_2 + extract.

suggested that seed extract pre-treatment markedly protected the cell death of 3T3-L1 cells. The result was consistent with previous studies, which have also affirmed the protective effects of quercetin against the oxidative stress [37].

Evaluation of ROS measurement in 3T3-L1 cells by confocal microscopy

The 3T3-L1 cells incubated with H_2O_2 showed a significant increase in ROS intensity (172 ± 4.29, $P < 0.05$) as compared

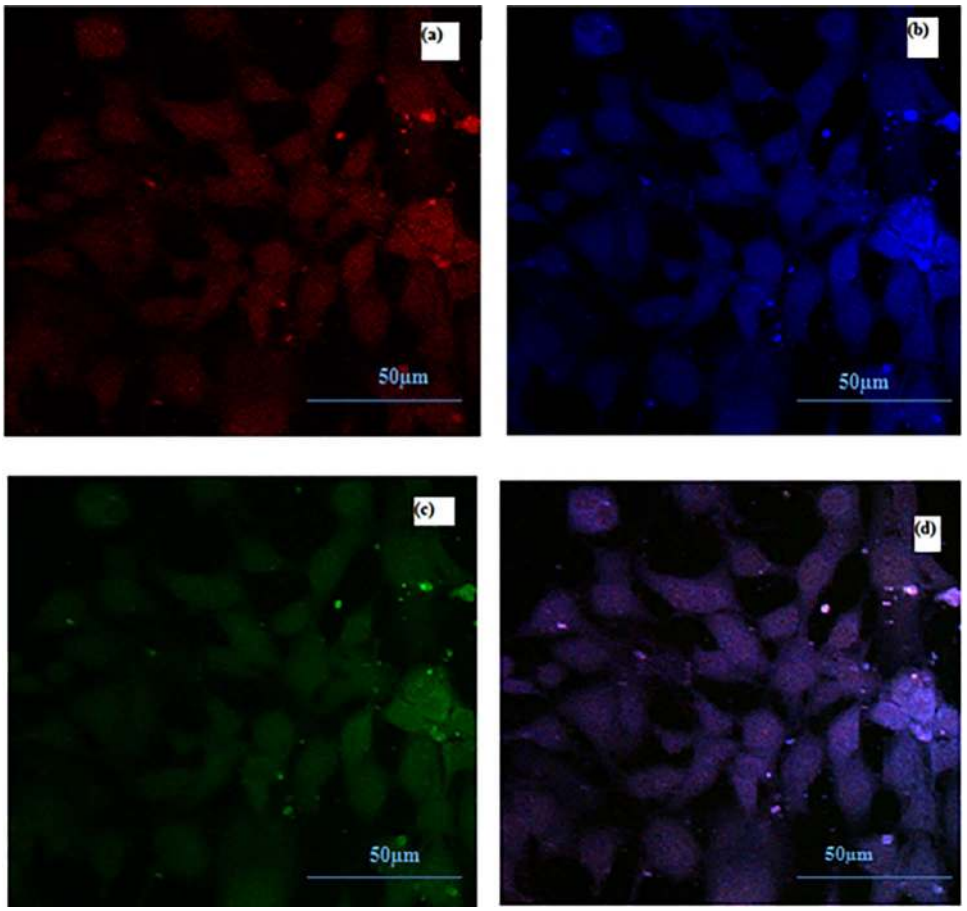

Figure 11: Confocal microscopy showing fluorescence signal represents apoptotic cells, apoptotic nuclei and strong ROS levels under combination of different dyes: (**a**) PI staining, (**b**) DAPI staining, (**c**) DCF staining and (**d**) Merged images of PI, DAPI and DCF.

Table 1: Quantitative analysis of nuclear change in 3T3-L1 cell population subjected to oxidative stress by PI staining

Samples	Number of apoptotic cells per 100 cells	Apoptotic ratio
Control	8 ± 0.04	0.08
Extract	10 ± 0.05	0.10
H_2O_2	35 ± 2.62	0.35
Extract + H_2O_2	26 ± 1.72	0.26

Table 2: Quantitative analysis of 3T3-L1 cell population subjected to oxidative stress by DAPI staining

Samples	Number of apoptotic cells per 100 cells	Apoptotic ratio
Control	7 ± 0.042	0.07
Extract	9 ± 0.065	0.09
H_2O_2	30 ± 2.54	0.30
Extract + H_2O_2	22 ± 1.64	0.22

to control (137 ± 2.64, $P < 0.05$). The cell in the presence of acetone extract showed lesser ROS intensity (143 ± 6.6, $P < 0.05$) than the H_2O_2-treated cells (Fig. 8). Phenols, in general flavonoids and phenylpropanoids, are oxidized by peroxidase and function in the H_2O_2-scavenging, phenolic/ASC/POX system [38]. Normal cells show a weak cytosolic and a somewhat stronger mitochondrial-type DCF fluorescence pattern, while apoptotic cells demonstrate strong diffuse fluorescence [39]. Furthermore, confocal microscopy results showed that FI was significantly increased after either insulin stimulation or H_2O_2 treatment in the 3T3-L1 cell line as evident from Fig. 8. Such results showed that H_2O_2, comparable to insulin therapy, can increase intracellular ROS production and alter the redox balance in 3T3-L1 cells [40]. ROS contribute to the progression of different human diseases, including type 2 diabetes mellitus (T2DM) [41]. ROS can inhibit insulin response and contribute to the development of insulin resistance, a crucial pathology of T2DM [41].

Qualitative and quantitative analyses of 3T3-L1 cells like apoptotic nuclei and apoptotic cell population by confocal microscopy

Some PI, DAPI and DCF population having cells have been shown to be apoptotic based on the characteristic morphology, including chromatin condensation, nuclear fragmentation, plasma membrane blebbing, condensed cytoplasm and dense bright green fluorescence as shown in Figs 9–11. The induction of apoptosis on 3T3-L1 cells was investigated by microscopic analysis of PI and DAPI. We observed numerous apoptotic cells with nuclear condensation and fragmentation (Figs 9 and 10). Table 1 indicated the effect of H_2O_2 on 3T3-L1 cells as it becomes permeable to PI,

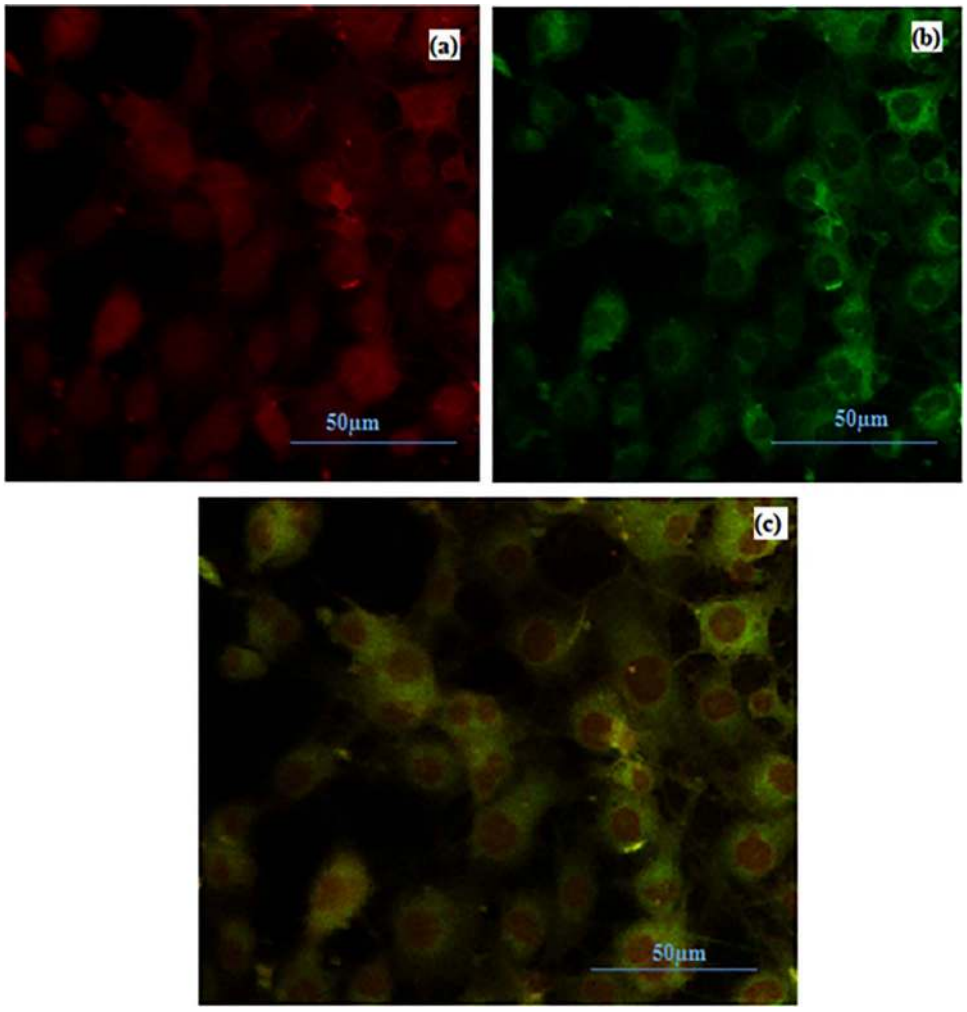

Figure 12: Oxidative stress cell population study under a combination of different dyes (confocal microscopy): (**a**) PI staining, (**b**) DCF staining and (**c**) merged images of PI and DCF.

and their % PI-positive (dead cell) populations were found to be $35 \pm 2.62\%$ ($P < 0.05$) with respect to control (Table 1). Control having % PI-positive was 0.08 ± 0.04 ($P < 0.05$). DAPI was used to visualize the nuclear DNA in both living and fixed cells. It also forms nonfluorescent intercalation complexes with double-stranded nucleic acids [42]. DAPI staining also confirmed that H_2O_2-treated cells increased the apoptotic nuclei concerning control. DAPI staining reported apoptotic nuclei having control, extract and H_2O_2 were found to be 7 ± 0.042, 9 ± 0.065 and $30 \pm 2.54\%$ ($P < 0.05$), respectively (Table 2). It was evident from (Tables 1 and 2) extract that it was efficient for reducing oxidative stress in terms of % apoptotic nuclei and % cell death. The reason for using PI and DAPI in tandem was to measure apoptosis and necrosis as DAPI enters all cells while PI only enters into necrotic cells or those undergoing late apoptosis (or secondary necrosis/necrosis) when membrane integrity is lost (Figs 11 and 12). Literature also supported that the findings regardless of the type of cell death, loss of membrane integrity is directly proportional to nuclear morphology in the same cell [43]. Researchers concluded that H_2O_2 therapy is responsible for causing a proliferation arrest that is directly or indirectly related to a rise in mitochondrial content of 3T3-L1 fibroblast cell-like pre-adipocytes with some large dietary polyphenols completely or partially shielding the cells against the oxidative stress. Researchers have supported that H_2O_2 treatment was responsible for inducing a proliferation arrest associated with an increase in mitochondrial content in 3T3-L1 preadipocytes, preconditioning with some major dietary polyphenols totally or partially that protects the cells against oxidative stress consequences [44].

Roughness study in 3T3-L1 cell line due to oxidative stress

H_2O_2 treatment roughness was maximum (182.5 ± 17.3 nm), and cells on treatment with H_2O_2 in combination with extract roughness decreased to 208 ± 12.2. Oxidative stress resulted in a decrease in the mean cell volumes of the 3T3-L1 cells (Table 3), whereas when the cells were exposed to H_2O_2 concentrations for 1 h, it raised the cell roughness but on treatment with the H_2O_2 extract, the effect was reversed (Fig. 13). Figure 13 indicated the formation of "cavities" on the cell surfaces as the H_2O_2 concentration was increased. The alteration in cell morphologies was due to the oxidative damages of cell membranes by oxidation of lipids and proteins that are well known to modify the membrane fluidity and permeability [45]. The findings indicated that oxidative stress was responsible for the rapid decrease of mean cell volumes, the decline of cell viabilities and the initial

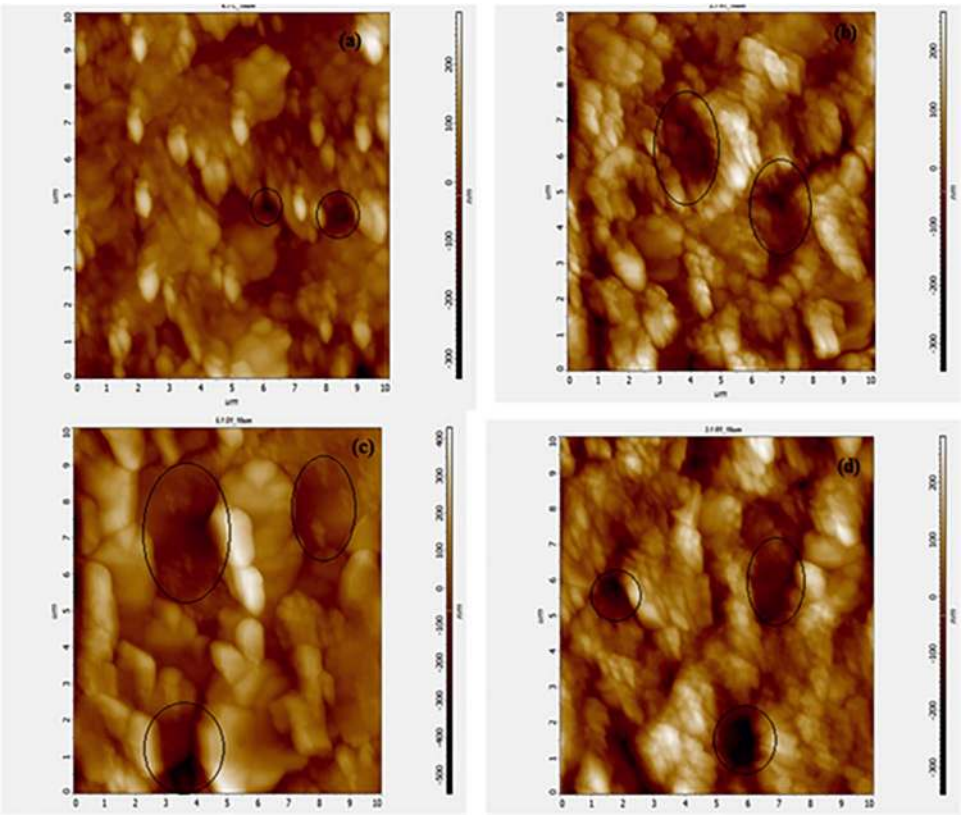

Figure 13: Atomic force microscopy shows cell roughness (nm) and mean cell volume (μm^3). (**a**) Control, (**b**) extract, (**c**) H_2O_2 and (**d**) extract + H_2O_2 (circle represents cavity).

Table 3: Analysis of cell roughness (nm) and mean cell volume (μm^3) of 3T3-L1 cell line having (a) control, (b) extract, (c) H_2O_2 and (d) extract + H_2O_2 by atomic force microscopy

Sample	Cell roughness (nm)	Mean cell volume (μm^3)
Control	120.8 ± 12.8	266 ± 16.4
Extract	134.8 ± 16.4	245 ± 15.6
H_2O_2	182.5 ± 17.3	208 ± 12.2
Extract + H_2O_2	162.32 ± 14.5	235 ± 14.8

compression of cell walls followed by the formation of cavities on cell surfaces, changes in cell morphologies and increase in surface roughness in the 3T3-L1 cell. The presence of polyphenols (phenolics, flavonoids or synergistic effect) in seed extract was responsible for cell roughness. Findings by other researchers also authenticated the observations made in the present study [46].

Oxidative stress analysis by SEM

Surface morphology (spanning topographic features) of cell image of treated and untreated was observed by SEM. The control showed fibroblast-like morphology (Fig. 14). Besides H_2O_2-treated cells exhibiting an altered morphology, as evident from Fig. 14, a larger and more irregular, three-dimensional (3D)-cuboidal or polygonal morphology was seen. Literature also authenticated that H_2O_2 treatment induces a proliferation arrest associated with an increase in mitochondrial content in 3T3-L1 preadipocytes [44]. Polyphenols are proficient to directly scavenge ROS and moreover induce the activation of Nrf2 that in turn leads to an activation of various antioxidant enzymes [47].

Evaluation of glucose uptake study in 3T3-L1 cell by confocal microscopy and flow cytometry

We examined changes in glucose uptake ability in 3T3-L1 cells by different types of seed extract such as aqueous, methanol and ethanol. When the comparison was made with 2-NBDG, it was found that it had better FI with acetone extract (0.86 ± 0.031) than with NBDG (0.45 + 0.016) (Fig. 15). The flow cytometry approach also revealed that 2-NBDG (2.08 ± 0.31) showed relative FI lesser than acetone (4.98 ± 0.62) and aqueous (3.52 ± 0.52) seed extract (Fig. 16). Higher relative FI is indicative of more glucose uptake by 3T3-L1 cells. PPARγ agonists are responsible for glucose transport by modulating the expression of several genes involved in glucose uptake [48]. Literature has also suggested that ethanol extract could promote glucose uptake in 3T3-L1 preadipocytes via the insulin signaling pathway [49].

Molecular docking

Both ligands were docked on target enzyme structure, XO, and consequently consistent docking poses were found. Moreover, the best and productive binding mode is recruited based on these main parameters: first, consistent ligand docking pose and

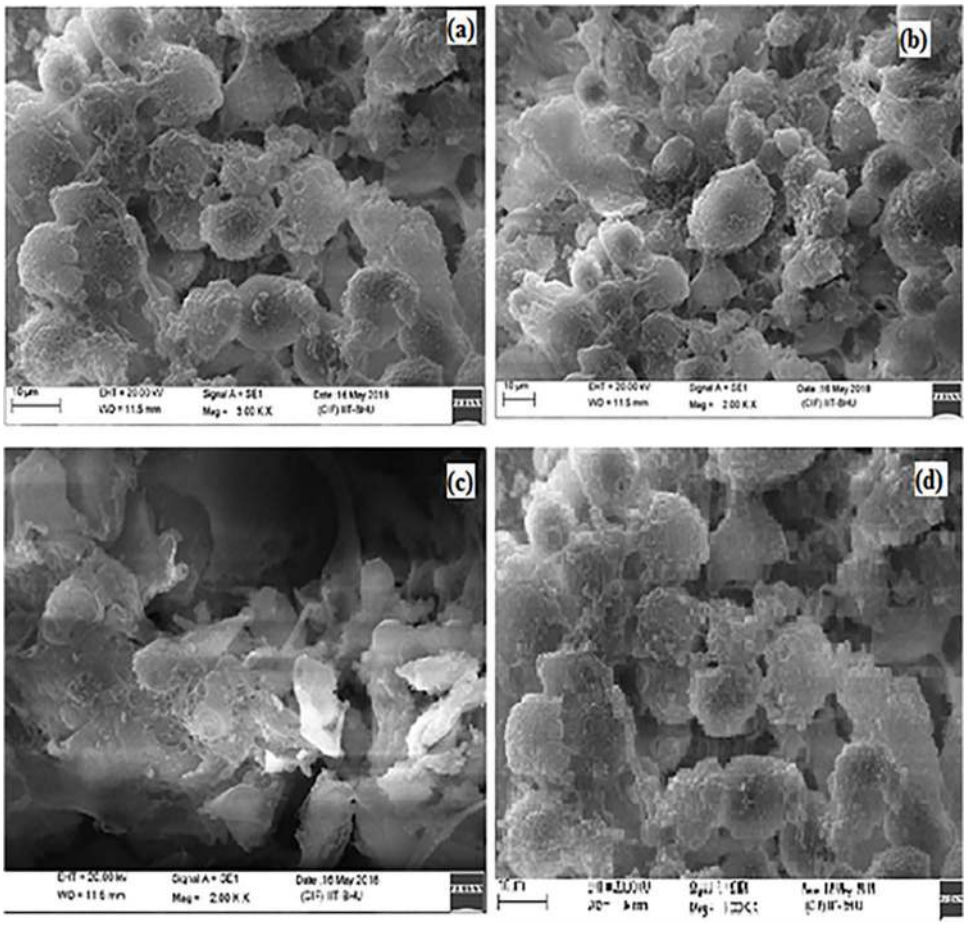

Figure 14: .SEM showing surface morphology of 3T3-L1 cell (oxidative stress study). (**a**) Control, (**b**) extract, (**c**) H_2O_2 and (**d**) H_2O_2 + extract.

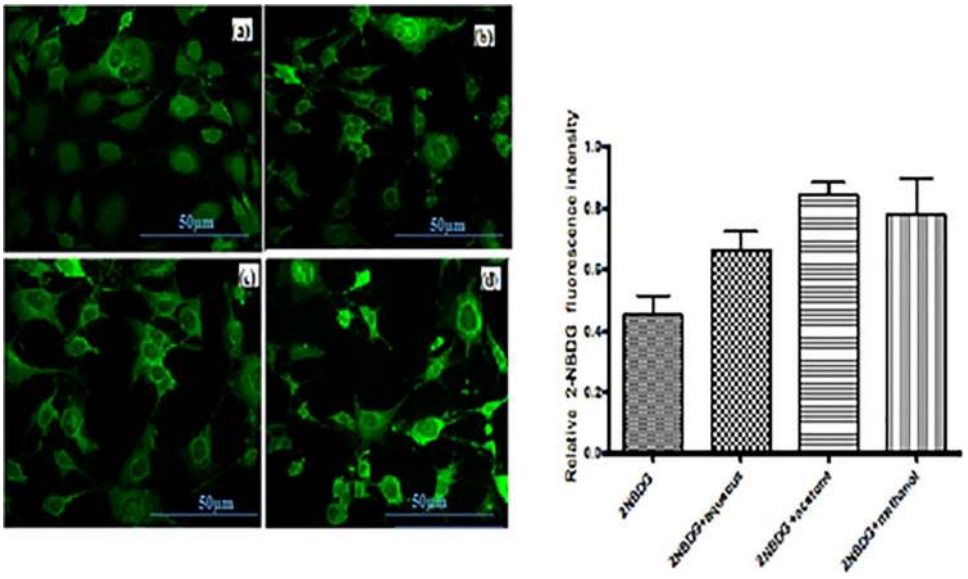

Figure 15: Measurement of glucose uptake by confocal microscopy in 3T3-L1. Cells were seeded in six-well plates and treated with 100 nM of insulin and 10 µM of 2-NBDG in the presence or absence of samples. (**a**) 2-NBDG, (**b**) aqueous seed extract, (**c**) acetone seed extract and (**d**) methanol seed extract (right side of image relative of FI measured by image J software).

possessing less binding energy on the target protein; second, protein residues were recruited by distance within less than 0.4 nm from ligands and third, the stability of the complexes in 20-ns MD simulations. Three docking trials were performed and a total of 10 binding poses were obtained in each trial. We selected acute five poses to show this work based on lower binding energy.

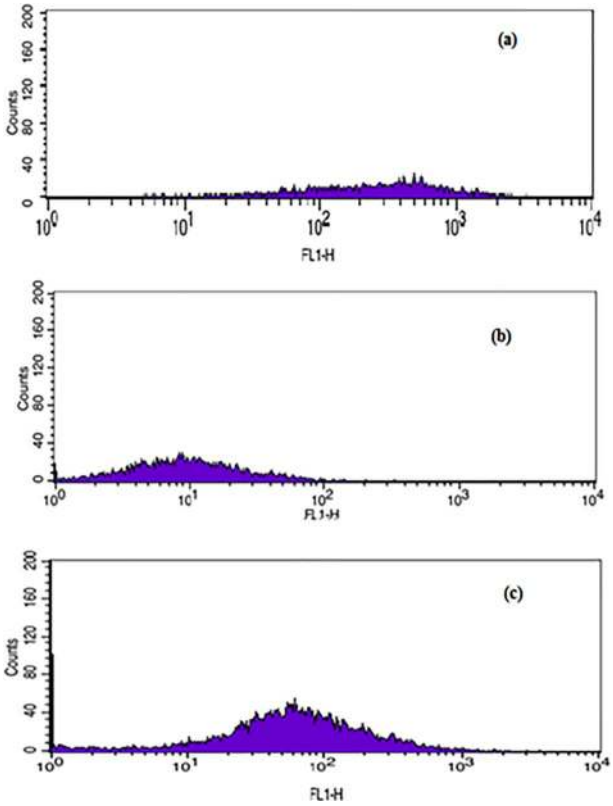

Figure 16: Evaluation of glucose uptake by flow cytometry in 3T3-L1. Cells were seeded in six-well plates and treated with 100 nM insulin and 10 µM 2-NBDG in the presence or absence of samples (50 µM) for 24 h. After incubation, cells were washed with PBS and 2-NBDG uptake was calculated by a flow cytometer. (**A**) Control, (**B**) aqueous seed extract and (**C**) acetone seed extract.

Table 4: Docking details of catechin and gallic acid on XO

Compounds	Binding energy (kJ/mol)	Detail of hydrogen bonds
Catechin	−8.54	1. Q1194:HE21-O:Cat 2. Cat:H-O:M1038 3. Cat:H-OE2:E1261 4. A1079:HN-O:Cat 5. Cat:H-OE1:Q1194
Gallic acid	−6.83	1. K1228:HZ2-O:Gal 2.R426:HH12-O:Gal 3. Gal:H-O:Q423 4. KHZ3-O:Gal 5. K433:HZ2-O:Gal

Therefore, the details of the top five binding poses, as well as the interaction profile of catechin and gallic acid, were concluded in Table 4. A best binding pose was chosen by considering less binding energy among the poses. We docked both ligands at the same active site to illustrate the comparative effects on the XO enzyme. The binding energy of the best pose was recovered as −9.93 and −6.83 kJ/mol for catechin and gallic acid, respectively (Table 4).

Table 5: List of system and simulations detail

Serial No	System	Ligand	PDB file	Duration (ns)	Repeats
1.	Apo: XO	Nil	1FIQ	10	1
2.	Cat:XO	Catechin	1FIQ	20	1
3.	Gal: XO	Gallic acid	1FIQ	20	1

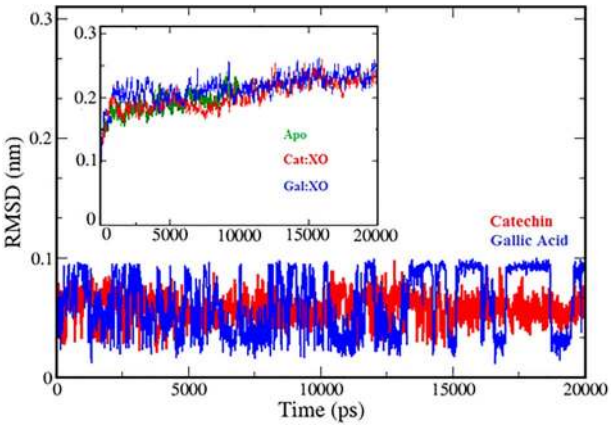

Figure 17: Backbone atom's RMSD calculations of catechin and gallic-acid compound (red and blue, respectively) are approximate. Furthermore, the RMSDs of each complex system are also depicted in the subplot. Green, red and blue color codes are assigned for apo (10-ns), Cat: XO and Gal: XO, respectively.

Molecular dynamics simulation study

The simulation was carried out for 10 ns for the apo state of XO whereas for the holo XO (XO + catechin, XO + gallic acid), catechin and gallic acid were simulated for a total of 20 ns. Table 5 reports the simulations performed in this study. Each of the simulations was initiated with randomly selected initial velocities. The total of 20-ns trajectory was used for analyses; consequently, it was observed that catechin (red line plot) was found stable and remained strictly within the binding pocket at the end of the simulation. The average value of RMSD for gallic acid was noted as 0.05 nm. However, the plot for gallic acid represents fluctuations during the entire simulation, with the average RMSD value as 0.048 nm. On the contrary, the considerable movement of gallic acid was found during the simulation; however, the movement had occurred within the binding pocket. To evaluate the quality of complexes and the apo state of enzyme, the RMSD values of the protein backbone atoms relative to the initial equilibrated structure during the phase of the simulation were calculated (plotted in Fig. 17). Each system reached equilibrium after ∼8 ns of the simulation phase; also, this result shows that the trajectories of the MD simulations for both complexes after equilibrium were reliable for postanalyses. Apo state of the enzyme means xanthine oxidase (10-ns simulation) and exhibits the same pattern RMSD has fluctuated within ∼0.18–0.23 nm. The molecular dynamics simulation indicated that the protein-ligand complex remains stable during the last 10 ns of the simulation. This study also showed that there was a shift in a ligand, which could be due to the change in binding type. Protein-ligand complexes (xanthin oxidase with catechin and gallic acid) exhibited approximately the same pattern after 10 ns, which suggests a conformational change during MD simulation.

Cluster analysis

The cluster approximations displayed the effect of ligands (catechin and gallic acid) on the XO enzyme employing temporal distribution. The trajectories were subjected to cluster analysis (cut-off value 0.15 nm) to secure convergence and observe the effect of both the ligands during the simulation. The large dominating clusters in the figure were in rapid equilibrium within 14 ns implying that the system was in fast equilibrium. For complex Cat: XO, initially there were ~7 clusters found, although, at the later simulation time, it resists up to ~1–2 clusters, which showed longer lifetime (Fig. 18). However, one cluster possessed a comparatively longer time (~14 ns). At the beginning of the simulation, maximum clusters for Gal: XO complex was classified up to 5 clusters; after ~5-ns time, it had acquired 2 leading clusters and the last one was showing longer lifetime, which was noted to be more than 10 ns (Fig. 18). Both complexes were executed less noisy, and trajectory exhibits a smooth continuous transition to a new conformation, represented by clusters. The cartoon representation of complex structures offered a location of catechin and gallic-acid ligand, and the enlarged view gives insight into the interaction residues and number of hydrogen bonds, which were formed during the simulation. The potential surface exhibits red, blue and white interfaces, a major negative lobe (red) and a smaller positive one (blue). The electrostatic interface of the enzyme surface indicates the total electrostatic area of interaction with ligand. In the case of catechin interacting amino acid residues, it covered mostly the positive potential; however, the negative lobe has also occupied some residues, whereas due to lesser molecular weight, gallic acid, the binding amino acid residues covered less surface area. Mostly, neutral (white) electrostatic lobe was found within the binding pocket of gallic acid. This presentation was fairly approximated by the level of 4 k_BT surface (Fig. 18) and bound to the protein the ligands were trapped within the deep energetic wells.

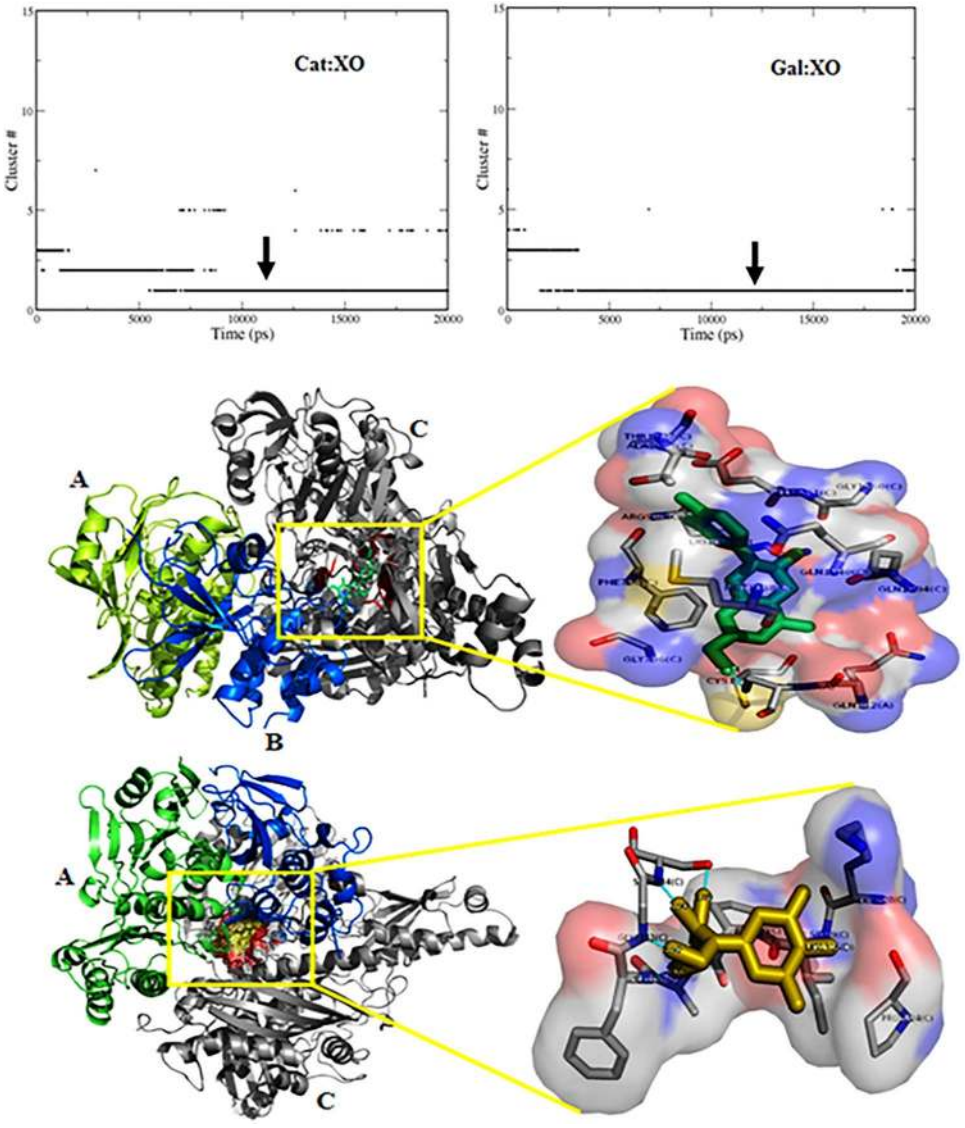

Figure 18: The size distribution of the clusters of both complex, simulated for 20 ns. The temporal distribution is presented for each complex for backbone atoms, using the same cut-off value (0.15 nm). The arrow marks the number of clusters that encompass 95% of all structures. Cartoon visualization of representative structure (upper panel: cat: XO and lower: gal: XO), magnifying the view depicts interacting residues within catechin (lime) and gallic acid (yellow) surrounded by a surface of the electrostatic potential, depicting as red (negative potential) and blue (positive potential). The cyan line shows the hydrogen bonding.

Conclusions

Dietary polyphenols from faba bean may be an alternative to medication for future prospects. Molecular docking described the probable binding poses with considerable binding energy, and the molecular dynamics simulations provided support of the effect of the ligands (catechin and gallic acid), in the active site of XO enzyme. Catechin and gallic-acid ligands were mostly trapped within the binding site and strictly bound with interacting residues within an appropriate electrostatic shell. The representative structure of the largest cluster illustrated about both the complexes. Findings may give an insight into the discovery of future drugs, which might be useful for oxidative stress treatment, and its consequences might be useful for diabetic disorders.

Conflict of interest statement

Authors declared no conflict of interest.

Acknowledgements

The authors express gratitude for the School of Biochemical Engineering, Indian Institute of Technology (BHU), Varanasi, India for providing infrastructure for research work, seed material for NBPGR New Delhi, confocal microscopy and flow cytometry for Interdisciplinary School of Life Sciences (ISLS) BHU, SAIF IIT Bombay, for mass spectrometry, Tel Aviv University, Israel for providing a computational facility for molecular dynamics simulation and also are grateful for the Central Instrument Facility Centre (CIFC)-IIT(BHU), Varanasi.

References

1. Newsholme P, Haber E, Hirabara S *et al*. Diabetes associated cell stress and dysfunction: role of mitochondrial and non-mitochondrial ROS production and activity *J Physiol* 2007;**583**:9–24.
2. Ceriello A, Motz E. Is oxidative stress the pathogenic mechanism underlying insulin resistance, diabetes, and cardiovascular disease? The common soil hypothesis revisited. *Arterioscler Thromb Vasc Biol* 2004;**24**:816–23.
3. Goel R, Bhatia D, Gilani SJ *et al*. Medicinal plants as antidiabetics, A review. *Int Bull Drug Res* 2012;**1**:100–7.
4. Patel D, Kumar R, Laloo D *et al*. Natural medicines from plant source used for therapy of diabetes mellitus: An overview of its pharmacological aspects. *Asian Pac J Trop Dis* 2012;**2**: 239–50.
5. Hemingway RW, Laks PE. *Plant Polyphenols: Synthesis, Properties, Significance*. Vol. 59. Springer Science & Business Media, 2012.
6. Baginsky C, Peña-Neira Á, Cáceres A *et al*. Phenolic compound composition in immature seeds of fava bean (Vicia faba L.) varieties cultivated in Chile. *J Food Compos Anal* 2013;**31**:1–6.
7. Turco I, Ferretti G, Bacchetti T. Review of the health benefits of Faba bean (Vicia faba L.) polyphenols. *J Food Nutr Res* 2016;**55**.
8. Sabu M, Smitha K, Kuttan R. Anti-diabetic activity of green tea polyphenols and their role in reducing oxidative stress in experimental diabetes. *J Ethnopharmacol* 2002;**83**:109–16.
9. Miric DJ, Kisic BM, Filipovic-Danic S *et al*. Xanthine oxidase activity in type 2 diabetes mellitus patients with and without diabetic peripheral neuropathy. *J Diabetes Res* 2016;**2016**.
10. Costantino L, Albasini A, Rastelli G *et al*. Activity of polyphenolic crude extracts as scavangers of superoxide radicals and inhibitors of xanthine oxidase. *Planta Med* 1992;**58**:342–4.
11. Lin S, Zhang G, Liao Y *et al*. Dietary flavonoids as xanthine oxidase inhibitors: structure-affinity and structure-activity relationships. *J Agric Food Chem* 2015;**63**:7784–94.
12. Yılmaz S, Ergün S. Effects on haematological, serum biochemical, non-specific immune and head kidney gene expression responses. *Fish Shellfish Immunol* 2018;**78**:140–57.
13. Gessner D, Ringseis R, Eder K. Potential of plant polyphenols to combat oxidative stress and inflammatory processes in farm animals. *J Anim Physiol Anim Nutr* 2017;**101**:605–28.
14. Shimoyama T, Yamaguchi S, Takahashi K *et al*. Gliclazide protects 3T3L1 adipocytes against insulin resistance induced by hydrogen peroxide with restoration of GLUT4 translocation. *Metabolism* 2006;**55**:722–30.
15. Anari MR, Sanchez RI, Bakhtiar R *et al*. Integration of knowledge-based metabolic predictions with liquid chromatography data-dependent tandem mass spectrometry for drug metabolism studies: application to studies on the biotransformation of indinavir. *Anal Chem* 2004;**76**:823–32.
16. Lee JS, Kim DH, Liu KH *et al*. Identification of flavonoids using liquid chromatography with electrospray ionization and ion trap tandem mass spectrometry with an MS/MS library. *Rapid Commun Mass Spectrom* 2005;**19**:3539–48.
17. Choudhary DK, Mishra A. In vitro and in silico interaction of faba bean (Vicia faba L.) seed extract with xanthine oxidase and evaluation of antioxidant activity as a therapeutic potential. *Nat Prod Res* 2018;1–5.
18. Nakashima N, Sharma PM, Imamura T *et al*. The tumor suppressor PTEN negatively regulates insulin signaling in 3T3-L1 adipocytes. *J Biol Chem* 2000;**275**:12889–95.
19. Keston AS, Brandt R. The fluorometric analysis of ultramicro quantities of hydrogen peroxide. *Anal Biochem* 1965;**11**:1–5.
20. Rashmi R, Kumar TS, Karunagaran D. Human colon cancer cells differ in their sensitivity to curcumin-induced apoptosis and heat shock protects them by inhibiting the release of apoptosis-inducing factor and caspases. *FEBS Lett* 2003;**538**: 19–24.
21. Sarker KP, Obara S, Nakata M *et al*. Anandamide induces apoptosis of PC-12 cells: Involvement of superoxide and caspase-3. *FEBS Lett* 2000;**472**:39–44.
22. Adya AK, Canetta E, Walker GM. Atomic force microscopic study of the influence of physical stresses on Saccharomyces cerevisiae and Schizosaccharomyces pombe. *FEMS Yeast Res* 2005;**6**:120–8.
23. Chen L-Q, Hou B-H, Lalonde S *et al*. Sugar transporters for intercellular exchange and nutrition of pathogens. *Nature* 2010;**468**:527.
24. Abu-Reidah IM, Ali-Shtayeh MS, Jamous RM *et al*. HPLC-DAD-ESI-MS/MS screening of bioactive components from Rhus coriaria L.(Sumac) fruits. *Food Chem* 2015;**166**:179–91.
25. Morris GM, Huey R, Lindstrom W *et al*. AutoDock4 and AutoDockTools4: Automated docking with selective receptor flexibility. *J Comput Chem* 2009;**30**:2785–91.
26. Van Der Spoel D, Lindahl E, Hess B *et al*. GROMACS: fast, flexible, and free. *J Comput Chem* 2005;**26**:1701–18.
27. Pronk S, Páll S, Schulz R *et al*. GROMACS 4.5: a high-throughput and highly parallel open source molecular simulation toolkit. *Bioinformatics* 2013;**29**:845–54.
28. Oostenbrink C, Villa A, Mark AE *et al*. A biomolecular force field based on the free enthalpy of hydration and solvation: the GROMOS force-field parameter sets 53A5 and 53A6. *J Comput Chem* 2004;**25**:1656–76.

29. Toukan K, Rahman A. Molecular-dynamics study of atomic motions in water. *Phys Rev B* 1985;**31**:2643.
30. Essmann U, Perera L, Berkowitz ML *et al*. A smooth particle mesh Ewald method. *J Chem Phys* 1995;**103**:8577–93.
31. Hess B, Bekker H, Berendsen HJ *et al*. LINCS: a linear constraint solver for molecular simulations. *J Comput Chem* 1997;**18**:1463–72.
32. Schüttelkopf AW, Van Aalten DM. PRODRG: a tool for high-throughput crystallography of protein-ligand complexes. *Acta Crystallogr D Biol Crystallogr* 2004;**60**:1355–63.
33. Lee RJ, Lee VS, Tzen JT *et al*. Study of the release of gallic acid from (–)-epigallocatechin gallate in old oolong tea by mass spectrometry. *Rapid Commun Mass Spectrom* 2010;**24**:851–8.
34. Yagi K, Kondo D, Okazaki Y *et al*. A novel preadipocyte cell line established from mouse adult mature adipocytes. *Biochem Biophys Res Commun* 2004;**321**:967–74.
35. Cheng Y-L, Chang W-L, Lee S-C *et al*. Acetone extract of Bupleurum scorzonerifolium inhibits proliferation of A549 human lung cancer cells via inducing apoptosis and suppressing telomerase activity. *Life Sci* 2003;**73**:2383–94.
36. Marimoutou M, Le Sage F, Smadja J *et al*. Antioxidant polyphenol-rich extracts from the medicinal plants Antirhea borbonica, Doratoxylon apetalum and Gouania mauritiana protect 3T3-L1 preadipocytes against H2O2, TNF*a* and LPS inflammatory mediators by regulating the expression of superoxide dismutase and NF-κB genes. *J Inflamm* 2015;**12**:10.
37. Nabavi SM, Nabavi SF, Eslami S *et al*. In vivo protective effects of quercetin against sodium fluoride-induced oxidative stress in the hepatic tissue. *Food Chem* 2012;**132**:931–5.
38. Michalak A. Phenolic compounds and their antioxidant activity in plants growing under heavy metal stress. *Pol J Environ Stud* 2006;15.
39. Shoaib A, Dixit RK, Badruddeen *et al*. Cure of human diabetic neuropathy by HPLC validated bark extract of Onosma echioides L. root. *Nat Prod Res* 2018;1–5.
40. Mahadev K, Wu X, Zilbering A *et al*. Hydrogen peroxide generated during cellular insulin stimulation is integral to activation of the distal insulin signaling cascade in 3T3-L1 adipocytes. *J Biol Chem* 2001;**276**:48662–9.
41. Tiganis T. Reactive oxygen species and insulin resistance: the good, the bad and the ugly. *Trends Pharmacol Sci* 2011;**32**:82–9.
42. Bringezu T, Sharbel T, Weber W. Grain development and endoreduplication in maize and the impact of heat stress. *Euphytica* 2011;**182**:363.
43. Darzynkiewicz Z, Bruno S, Del Bino G *et al*. Features of apoptotic cells measured by flow cytometry. *Cytometry* 1992;**13**:795–808.
44. Baret P, Septembre-Malaterre A, Rigoulet M *et al*. Dietary polyphenols preconditioning protects 3T3-L1 preadipocytes from mitochondrial alterations induced by oxidative stress. *Int J Biochem Cell Biol* 2013;**45**:167–74.
45. Rueda-Jasso R, Conceiçao LE, Dias J *et al*. Effect of dietary non-protein energy levels on condition and oxidative status of Senegalese sole (Solea senegalensis) juveniles. *Aquaculture* 2004;**231**:417–33.
46. Daw AE, Kazi HA, Colombo JS *et al*. Differential cellular and microbial responses to nano-/micron-scale titanium surface roughness induced by hydrogen peroxide treatment. *J Biomater Appl* 2013;**28**:144–60.
47. Surh Y-J, Kundu JK, Na H-K. Nrf2 as a master redox switch in turning on the cellular signaling involved in the induction of cytoprotective genes by some chemopreventive phytochemicals. *Planta Med* 2008;**74**:1526–39.
48. Picard F, Auwerx J. PPARγ and glucose homeostasis. *Annu Rev Nutr* 2002;**22**:167–97.
49. Takahashi M, Takahashi Y, Takahashi K *et al*. Chemerin enhances insulin signaling and potentiates insulin-stimulated glucose uptake in 3T3-L1 adipocytes. *FEBS Lett* 2008;**582**:573–8.